18 (2026) 100256

Contents lists available at ScienceDirect

Superconductivity

journal homepage: www.elsevier.com/locate/supcon

Research Article

Berezinskii-Kosterlitz-Thouless to BCS-like superconducting fluctuation crossover driven by weak magnetic fields in ultra-thin NbN films

Meenakshi Sharma [a,b], Sergio Caprara [c], Andrea Perali [d,*], Surinder P. Singh [e], Sandeep Singh [e], Matteo Fretto [f], Natascia De Leo [f], Nicola Pinto [a,f]

[a] School of Science and Technology, Physics Division, University of Camerino, Via Madonna delle Carceri 9, 62032, Camerino, MC, Italy
[b] Quantum Information for Quantum Materials, Max Planck Institute for Chemical Physics of Solids, Nothnitzer Strasse 40, 01187, Dresden, Saxony, Germany
[c] Dipartimento di Fisica, "Sapienza" Università di Roma, Rome, Italy
[d] School of Pharmacy, Physics Unit, University of Camerino, Via Madonna delle Carceri 9, 62032, Camerino, MC, Italy
[e] CSIR-National Physical Laboratory, Dr. K.S. Krishnan Marg, 110012, New Delhi, India
[f] Advanced Materials Metrology and Life Science Division, INRiM, Strada delle Cacce 91, 10135, Torino, Italy

A R T I C L E I N F O

Keywords:
2D superconductivity
NbN nanofilms
BKT transition
Electronic transport measurements

A B S T R A C T

The Berezinskii-Kosterlitz-Thouless (BKT) transition in ultra-thin NbN films is investigated in presence of weak perpendicular magnetic fields. A jump in the phase stiffness at the BKT transition is detected up to 5 G, while the BKT features are smeared between 5 G and 50 G, disappearing altogether at 100 G, where conventional current-voltage behavior is observed. Our findings demonstrate that weak magnetic fields, insignificant in bulk systems, deeply affect our ultra-thin films, promoting a crossover regime from the Halperin-Nelson fluctuations to the BCS-like state with Ginzburg-Landau fluctuations, as the field increases. This behavior is related to field-induced free vortices that screen the vortex-antivortex interaction and smear the BKT transition.

1. Introduction

In low-dimensional superconducting (SC) systems, the interplay between quantum coherence, interactions, and topology can give rise to unexpected emergent quantum phenomena. A clean two-dimensional (2D) superconductor undergoes a Berezinskii-Kosterlitz-Thouless (BKT) phase transition [1–7], characterized by the proliferation of thermally activated vortex-antivortex pairs, an abrupt jump in the superfluid stiffness, and the disruption of the quasi-long-range-ordered SC state. This ultimately leads to the formation of a pseudogap above the transition temperature [8,9]. BKT physics has been experimentally observed in numerous ultra-thin SC films [5,10–14].

Despite this extensive body of work, the effects of low magnetic fields ($H \sim H_{c1}$, where H_{c1} denotes the lower critical magnetic field) remain insufficiently explored, even though they are of central importance for 2D SC systems. Existing studies [4,10,15,16] indicate that the SC properties of 2D systems can be significantly altered even at weak magnetic fields, due to factors such as inhomogeneity, disorder, vortex pinning mechanisms, edge vortices, and topological defects [15,17].

A comprehensive experimental investigation of magnetic field effects on the BKT transition in SC nanofilms, such as indium/indium oxide composites, was reported by Garland and Lee in Ref. [18]. In these systems, the pinning of field-induced vortices plays a crucial role in modifying the BKT transition. At finite magnetic fields, a small but finite resistance persists below the BKT transition temperature T_{BKT}, preventing the system from reaching a true zero-resistance state. Nevertheless, a pronounced change in the temperature dependence of the resistance is observed as the system approaches T_{BKT} from above, manifesting experimentally as a crossover scale that separates two qualitatively distinct transport regimes. This crossover scale, as well as the physics above it, was found to be nearly independent of the applied magnetic field. Closer examination, however, suggests that the system studied in Ref. [18] differs substantially from NbN in terms of the relevant parameter regimes and the degree of disorder, which, in turn, are reflected in the different behavior of our samples. Specifically, Garland and Lee reported a resistive tail occurring at resistivity values an order of magnitude lower than ours and a magnetoresistance pointing to an activated temperature dependence due to vortex pinning. In our NbN samples, because of high morphological and structural quality, the pinning effects are excluded.

Indeed, in contrast with the findings of Garland and Lee, we demonstrate here that NbN SC nanofilms exhibit a nontrivial evolution of the BKT physics under weak magnetic fields when approaching T_{BKT} from above, with a gradual change in the critical fluctuations, from Gaussian-like to topological.

* Corresponding author.
E-mail address: andrea.perali@unicam.it (A. Perali).

https://doi.org/10.1016/j.supcon.2026.100256
Received 16 December 2025; Received in revised form 15 April 2026; Accepted 16 April 2026
Available online 17 April 2026

We point out that, in real SC systems, several additional effects emerge when the film thickness d is reduced to values comparable to the coherence length ξ ($d \approx \xi$). These include, for instance, the appearance of resistive tail-like features, reported by several groups [10,14,19], which are commonly attributed to enhanced granularity [20,21], inhomogeneity, and vortex pinning effects [22]. Moreover, it has been argued that H_{c1} vanishes in granular 2D SC systems [18,23,24], leading to the generation of a large density of free vortices even at very weak perpendicular magnetic fields. These vortices can readily penetrate the material and strongly interact with thermally generated vortex-antivortex pairs, thereby modifying the dynamics of the BKT transition.

To elucidate these complex interactions, we performed a systematic experimental study of the SC properties of NbN ultra-thin films. These systems constitute a particularly suitable platform for exploring the low-field regime [3,5,14,25], enabling us to investigate the fate of the BKT transition and its evolution under weak magnetic fields in the range 3–150 G. Our focus is on non-universal yet physically relevant features that influence transport properties in the fluctuation regime close to the BKT transition. These include the sharp jump of the exponent characterizing the nonlinear I–V response (associated with the emergence of superfluid stiffness below T_{BKT} in zero field), the characteristic temperature scale for the abrupt drop in resistivity (identified with T_{BKT} at zero field), and the behavior of the resistivity above this scale. We do not propose a new theoretical framework; the theory describing magnetic-field effects on the BKT transition has already been developed in detail in Refs. [26–28]. Rather, we focus on crossover phenomena occurring in the fluctuation regime, where the magnetic field does not completely obscure BKT physics.

In this context, we find that the established zero-field fluctuation theories—namely the Halperin-Nelson [29] and Aslamazov-Larkin [30] approaches—provide an accurate description of the phenomenology observed in our experiments. It is worth emphasizing that, although the formal expressions for the paraconductivity in the two theories are essentially identical (up to numerical prefactors) when written in terms of the characteristic fluctuation length scale, a crucial distinction emerges in their temperature dependence. Specifically, this length scale diverges algebraically in the Aslamazov-Larkin framework, while it exhibits an exponential divergence in the Halperin-Nelson theory. This difference reflects the distinct physical origins of the two approaches: Aslamazov-Larkin theory describes paraconductivity arising from Gaussian, amplitude-driven SC fluctuations, whereas Halperin-Nelson theory captures the non-Gaussian, phase-driven vortex-antivortex unbinding mechanism underlying the BKT transition. In our system, both regimes are relevant, and their interplay becomes particularly significant under the application of a magnetic field, which tends to suppress BKT features and promote a crossover toward an Aslamazov-Larkin (Ginzburg-Landau-like) fluctuation regime. Finally, we emphasize that NbN was chosen as an ideal experimental platform [14,25] due to its well-established dimensional crossover from three-dimensional (3D) to 2D behavior when the film thickness is reduced below the SC coherence length. This crossover naturally favors the emergence of vortex-antivortex pairs, making NbN an excellent system for investigating BKT physics.

2. Experimental details

The deposition of NbN nanofilms was carried out by using a reactive DC magnetron sputtering system (Excel Instruments), operational at the CSIR-National Physical Laboratory (NPL), India. The process utilized a 2-inch niobium target with a purity of 99.95%, positioned 8.5 cm away from the substrate. The sputtering atmosphere comprised N_2 and Ar gases (purity 99.999%). The deposition process was carried out on four substrate types: MgO, Si, and Al_2O_3 both r-and c-cut. Prior to deposition, each substrate was cleaned using acetone and isopropyl alcohol (IPA). The deposition chamber was evacuated at 10^{-7} mbar and substrates heated up at 600°C, before injecting N_2 and Ar gases at a ratio of 1:6, keeping the pressure constant at 7×10^{-3} mbar. A self-sustained plasma was formed at 20 W of dc power supply. A pre-sputtering of the target was performed for ≈ 2 min, then followed by deposition of NbN films. The deposition rate was found to be 0.3 nm/s and the thickness of the film was measured using a stylus profilometer (NanoMap 500ES). The surface topography of thin films of NbN deposited on an MgO substrate, was carefully characterized by atomic force microscopy (AFM) operated in tapping mode. Measurements were performed using a silicon AFM probe (Tap 300Al-G; resonant frequency ~ 300 kHz, force constant ~ 40 N/m) on a Multimode V AFM system (Veeco Instruments). For measurement of electrical transport properties, an 8-contacts geometry was chosen for the Hall bar fabrication, designed by the LibreCAD software. The fabrication steps involved spin coating (at 4000 rpm) of the photoresist (AZ 5214E) onto deposited films. A soft bake at 110°C for 3 min, resulted in a photoresist layer 1.4 μm thick. The pattern generation process involved a Karl Suss mask aligner (mod. MJB3) for optical lithography (line-space resolution of 2.5 μm) followed by wet chemical development to define the final geometry of the NbN Hall bars. In particular, the etching process was carried out by using deep reactive ion etching (RIE: PlasmaPro 100 Cobra Inductively Coupled Plasma Etching System, Oxford Instruments). The applied RIE powers were 30 W (table power rf) and 500 W (ICP power rf). Optimization of the fabrication parameters resulted in a mixture of CF_4 and Ar with fluxes of 90 and 10 sccm, respectively, at an operating pressure of 50 mTorr. All the samples were cleaned with a light-oxygen plasma before the etching process. The fabricated NbN devices on small PCBs were glued to a copper disk. Finally, thin Al wires were bonded to the Hall bar and PCB pads, allowing electrical connection to the measuring equipment.

Transport measurements were carried out in a He closed-cycle (liquid-free) cryostat (Advanced Research System mod. DE210) equipped with two Si diode thermometers (Lakeshore mod. DT-670) one out of two calibrated (maximum uncertainty of 6.3 mK) and used to read the film temperature by one channel of a source-measure unit (SMU, Keysight mod. B2912A). No change in the T value was detected under the perpendicularly applied magnetic field, in the intensity range used in our study.

The resistivity as a function of the temperature, $\rho(T)$, and the current-voltage ($I-V$) characteristics have been measured as a function of temperature. For the investigation of $\rho(T)$, the SMU has been operated in dc or pulsed mode. The latter (so-called delta mode) is based on the suitable combination of three consecutive current pulses of alternate polarity, virtually capable of minimizing thermoelectric forces and offsets otherwise affecting low-voltage detected values [31]. Current (in the range 1 μA–10 mA for $I-V$; typically $\leq 1\ \mu$A for ρ) has been sourced along the Hall bar length and the voltage drop detected by using two of three side contacts.

Electrical transport has started from the lowest T reached by the system (≈ 4.5 K), without any thermal stabilization of the device, exploiting the high thermal inertia of the cryostat, resulting in effective isothermal conditions of measure. In particular, the number of data points to average has been suitably chosen to keep the variation of the sample temperature as low as possible: $\lesssim 1$ mK, during data acquisition of the SC transition; $\lesssim 10-20$ mK, for $I-V$ characteristics.

During the $I-V$ measurements, we used a fast pulsed sweep technique utilizing a specific feature of the SMU. The current sourced to films comprised a ramp of pulses (1.1 ms of duration), with increasing intensity spanning several orders of magnitude, up to ≈ 1 mA. Between consecutive pulses, the current was switched off for ≈1 ms to minimize thermal effects. The entire $I-V$ measurement sequence was completed in approximately 5 s. This unconventional pulsed technique is expected to significantly reduce energy transfer to the sample by a factor of approximately 1000 compared to conventional continuous $I-V$ measurements thus minimizing any possible artifact related to sample heating.

To investigate the effects of weak perpendicular H fields on BKT physics in our NbN films, we examined the resistivity $\rho(T)$ behavior near the SC critical temperature T_c (see Section 3 for an operative def-

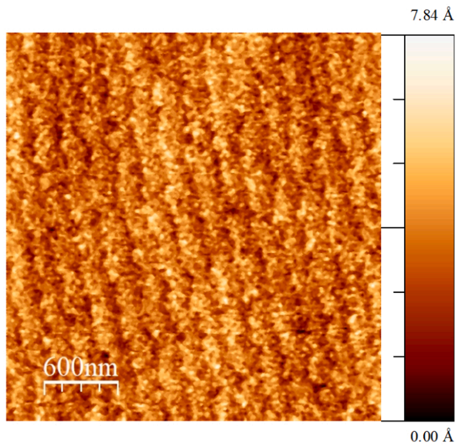

Fig. 1. Atomic Force Microscopy topography of a 10 nm-thick NbN film deposited on a MgO substrate. The root-mean-square (RMS) roughness of the scanned area ($3 \times 3\ \mu m^2$ wide) is 0.0984 nm.

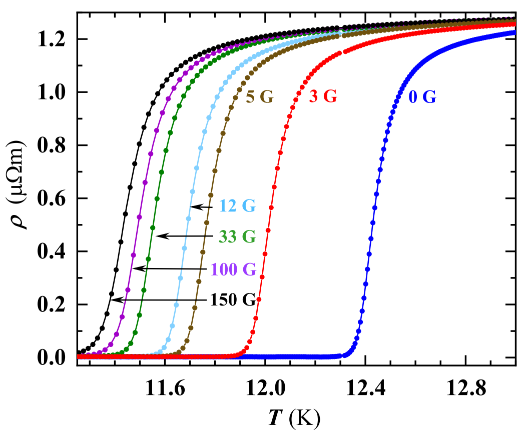

Fig. 2. Temperature dependent resistivity around the SC transition for a 10 nm-thick NbN film deposited on MgO (MO10), under several H field intensities applied perpendicular to the film surface. Experimental data (dots) are connected by B-spline lines.

inition of this quantity) under various applied H field intensities. H fields ranging from 3 G to 150 G were generated by a Bruker mod. B-E15v electromagnet, with the field direction perpendicular to the film surface. Both the H field intensity and its uniformity within an area of about 80 cm^2 were carefully monitored using an AlphaLab Inc. GM-2 gaussmeter with a sensitivity of 0.1 G (see Supplementary Material for additional and detailed information).

3. Results

As discussed in the Introduction, the SC properties of 2D systems can be strongly influenced by inhomogeneity, topological defects, and film morphology. To assess the morphological quality of the investigated NbN films, AFM analysis was performed. The films exhibit a highly uniform, continuous, and atomically smooth surface characterized by well-defined terrace-like features (see Fig. 1). Such terrace morphology is indicative of a step-flow growth mechanism and reflects the crystallographic step structure of the underlying MgO substrate, thereby confirming quasi-epitaxial growth of the NbN layer and its reduced roughness ($\lesssim 0.1$ nm; Fig. 1). Further details regarding the growth mechanism and morphological properties of the NbN films are provided in the Supplementary Material.

Strictly speaking, a true zero-resistance state is not achieved in the presence of a finite magnetic field. Nevertheless, the main features of the SC transition — most notably the pronounced drop in $\rho(T)$, upon decreasing the temperature below a characteristic scale — remain clearly visible and well defined within the low-field regime investigated here. For this reason, and for clarity, we adopt the same notation and terminology used in the zero-field case to denote the various characteristic temperature scales identified in our experiments.

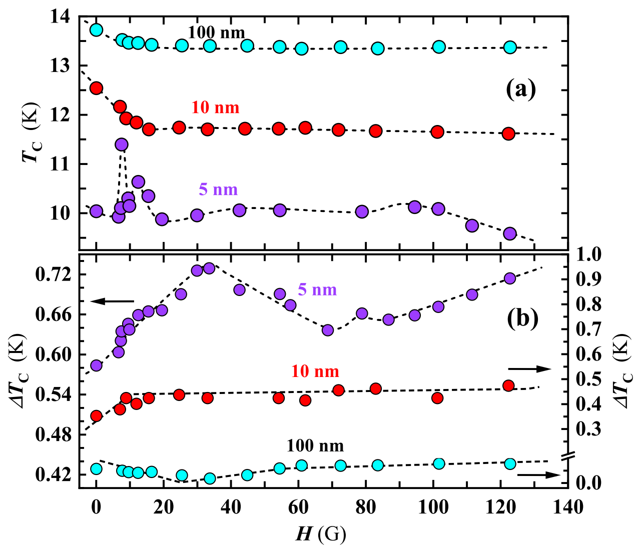

Fig. 3. Variation of T_c (a) and of the SC transition width (b) as a function of H for NbN films of diverse thickness. Symbol size exceeds error bar dimension. Dashed lines are guides to the eye.

The analysis of $\rho(T)$ in the vicinity of the SC critical temperature T_c reveals a strong dependence on the applied magnetic field H, characterized by a pronounced downward shift of T_c already at fields as low as 3 G. This suppression persists up to approximately 33 G (see Fig. 2). This unusually strong and non-monotonic shift of T_c at such weak magnetic fields highlights the peculiar nature of the investigated NbN thin films. In our analysis, T_c is defined as the midpoint between the temperatures corresponding to 10% ($T_{10\%}$) and 90% ($T_{90\%}$) of the normal-state resistivity $\rho(T)$, evaluated across the SC-to-normal transition and located on the resistivity plateau [32]. The difference between these two temperatures defines the transition width, $\Delta T_c = T_{90\%} - T_{10\%}$. Above the threshold field of approximately 33 G, the downward shift of T_c progressively weakens. This behavior can be ascribed to the increasing density of vortices induced by the applied magnetic field. Indeed, for a 10 nm thick NbN film, the lower critical field is estimated as $H_{c1} = 4\phi_0 \ln(w/\xi)/w^2 \approx 0.3$ G, where ϕ_0 is the magnetic flux quantum and $w = 50\ \mu m$ is the sample width [24]. As a consequence, the density of field-induced vortices, $n_f = H/\phi_0$, increases from approximately $1.45 \times 10^7\ cm^{-2}$ to $7.25 \times 10^8\ cm^{-2}$ as H is raised from 3 G to 150 G. Even the lowest applied field thus exceeds the estimated H_{c1} by more than one order of magnitude, favoring the nucleation of a sizable vortex population and leading to a substantial suppression of T_c. These findings are consistent with previous experimental studies [3] and numerical analyses addressing the interplay between sample width and coherence length [33]. In particular, a necessary condition for vortex generation, $w > 4.4\,\xi(T)$, was proposed in Ref. [34], and phase diagrams accounting for vortex nucleation at very low magnetic fields were obtained for large w/ξ ratios [23,33]. Small anomalies observed in sample MO10 around $H \approx 10$ G, affecting both T_c and ΔT_c, are also detected in thinner films ($d = 5$ nm, MO5) [14,35,36].

Remarkably, in the thinnest sample (MO5), a resonance-like enhancement of T_c is observed up to approximately 20 G, followed by a saturation regime extending to about 90 G, and a further decrease at higher fields (Fig. 3a). By contrast, in the thickest film (MO100, $d = 100$ nm), the influence of the magnetic field on T_c is strongly reduced: T_c shifts

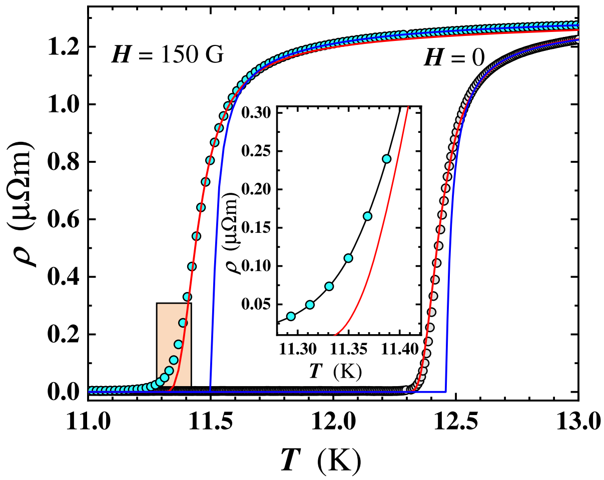

Fig. 4. Temperature dependence of the resistivity for MO10, at $H = 0$ G and $H = 150$ G. Lines are least squares fits by the Halperin-Nelson equation [Eq. (2), red] and by the Aslamazov-Larkin equation [Eq. (1), blue]. Smearing of the BKT phenomenon occurs at higher H fields. Inset: magnification of the region near the SC transition, highlighted by the orange rectangle.

by only ~ 0.2 K up to 20 G and remains essentially constant at higher fields (Fig. 3a). This behavior reflects the crossover from 2D to 3D superconductivity with increasing thickness, accompanied by the progressive suppression of BKT physics, which is consistently observed in all transport properties of this film. Furthermore, a pronounced non-monotonic dependence of the transition width ΔT_c on H is found in MO5, exhibiting an oscillatory behavior as a function of the magnetic field (Fig. 3b). For films with thicknesses of 10 nm (MO10) and 100 nm (MO100), variations in ΔT_c are confined to fields below approximately 15 G, with an overall much weaker effect in the thicker samples. This marked thickness dependence of the low-field SC response is attributed to the enhanced disorder inherent to films with thickness comparable to the coherence length ($\xi \approx 5$ nm). As the thickness increases toward 100 nm, SC fluctuations are progressively suppressed due to the 2D-3D crossover [9] and the concomitant reduction of disorder, as clearly observed in MO100 (Fig. 3b). In ultra-thin films, instead, the downward shift of T_c occurs predominantly at very low magnetic fields, indicating a crucial role played by the first field-induced vortices in enhancing fluctuations and weakening vortex-antivortex interactions. The microscopic origin of the ~ 2 K resonance-like enhancement of T_c observed in MO5 at extremely weak fields remains an open question. We argue that a complex interplay between disorder, coherence, and magnetic length scales may give rise to nonlinear effects in vortex-antivortex interactions, ultimately leading to an apparent amplification of T_c.

To further investigate the occurrence of the BKT transition, we analyzed the temperature dependence of the resistivity of sample MO10 in the vicinity of the SC transition, revealing several distinctive features. The normal-state resistivity was fitted at the highest applied field, $H = 150$ G, using a high-temperature expansion that avoids assumptions on the specific scattering mechanisms active in the system: $\rho_N(T) = A + B/T + C/T^2 + D/T^3$, in the interval $[T_1, T_2]$, with $T_c < T_1 < T_2$. We took $T_1 = 14$ K and $T_2 = 19$ K (see Figure S1). This protocol of using the same normal-state resistivity at all magnetic fields reduces the number of fitting parameters, at the expense of having slightly less accurate fits at low magnetic fields. The resulting least squares fitted parameters are: $A = 1.65 \times 10^{-6}\ \Omega\cdot$m, $B = -1.73 \times 10^{-5}\ \Omega\cdot$m$\cdot$K, $C = 3.02 \times 10^{-4}\ \Omega\cdot$m$\cdot$K^2, $D = -1.83 \times 10^{-3}\ \Omega\cdot$m$\cdot$K^3. A relevant quantity is the T dependent excess conductivity due to SC fluctuations, $\Delta\sigma = \sigma(T) - \sigma_N(T)$, where $\sigma_N(T) = [\rho_N(T)]^{-1}$ is the normal state conductivity. The experimental paraconductivity is defined in terms of the measured resistivity as $\Delta\sigma_{\rm exp}(T) = [\rho(T)]^{-1} - [\rho_N(T)]^{-1}$. We point out that, since the experimental conductivity becomes very large at the SC transition, any uncertainty on the (much smaller) normal-state conductivity becomes immaterial when the transition is approached.

Table 1
Parameters derived by the least square fitting of the sheet resistance data of film MO10, by using the Cooper-pair fluctuation models [i.e., Eqs. (1) and (2)] for some selected H intensities.

H (G)	$T_{\rm AL}$ (K)	s	$a_{\rm HN}$	$b_{\rm HN}$	$T_{\rm HN}$ (K)
0	12.46	0.075	0.0050	0.68	12.285
7	12.07	0.057	0.0048	0.68	11.88
50	11.62	0.029	0.0048	0.72	11.42
100	11.55	0.032	0.0048	0.72	11.35

The Aslamazov-Larkin paraconductivity is

$$\Delta\sigma_{\rm AL}(T) = \frac{1521}{s\,\sinh(\epsilon/s)} \tag{1}$$

where $1521\ (\Omega\cdot{\rm m})^{-1} = e^2/(16\hbar d)$ is the prefactor for $d = 10$ nm (MO10), and $\epsilon = \ln\left(T/T_{\rm AL}\right)$, with $T_{\rm AL}$ the critical temperature if the fluctuation regime was governed by amplitude fluctuations of the order parameter. The high-T dimensionless cutoff s, possibly related to the pseudogap in a system where the T scale for pair formation and phase coherence are sizably different [37], and $T_{\rm AL}$ are used as fitting parameters. We point out that the Aslamazov-Larkin behavior in 2D is universal (below a cutoff scale for the suppression of the fluctuations, that was absent in the original theory, but must likely occurs in real systems), in the sense that the prefactor for the leading contribution only depends on universal constants and the geometrical thickness of the sample d.

The Halperin-Nelson paraconductivity is

$$\Delta\sigma_{\rm HN}(T) = [\rho_N(T)]^{-1} a_{\rm HN} \sinh\left[\frac{b_{\rm HN}\left(T_{\rm HN}\right)^{1/2}}{\left(T - T_{\rm HN}\right)^{1/2}}\right] \tag{2}$$

where the temperature $T_{\rm HN}$ and the dimensionless parameters $a_{\rm HN}$ and $b_{\rm HN}$ are taken as fitting parameters. To keep our assumptions to a minimum, we rely on a form of the Halperin-Nelson paraconductivity that does not explicitly contain the mean-field critical temperature, since this latter quantity is ill-defined in the experiments, as opposed to the robust exponential dependence when $T_{\rm HN}$ is approached. To plot the Halperin-Nelson and Aslamazov-Larkin paraconductivity in the same plot, which is a function of $\epsilon = \ln(T/T_{\rm AL})$, we use the identity $T - T_{\rm HN} = T_{\rm AL}\,{\rm e}^{\epsilon} - T_{\rm HN}$.

Except at $H = 0$, $a_{\rm HN}$ is constant while $b_{\rm HN}$ exhibits a minor dependence on H (see Table 1). Regarding $T_{\rm AL}$ and $T_{\rm HN}$ both decrease monotonically with H, while $T_{\rm AL} - T_{\rm HN} \approx 0.2$ K in the entire H range (Table 1).

For $H = 0$, $\rho(T)$ is well fitted by Eq. (2), showing a clear manifestation of the BKT behavior. In our NbN system, we have not detected any tailing in the resistivity curve below the BKT transition within the resistivity range and temperature dependence regime discussed in Refs. [38–40]. Instead, below T_{BKT} we observe only a residual resistivity plateau that exhibits no evident temperature dependence.

However, under an applied H field, Eq. (2) gradually fails to fit the data, both close T_c, where a magnetic-field-driven foot develops, and further away from the transition, where the data are much better described by the Aslamazov-Larkin theory (Eq. (1), Fig. 4). We point out that there was no way to significantly improve the fitting by considering a Maki-Thomson contribution, presumably because this is suppressed by strong dephasing [41]. This gradual suppression of the BKT physics provides clear evidence for the contribution of H-induced vortices, even at extremely weak H fields, significantly screening the logarithmic interaction between vortex-antivortex pairs, thus affecting the dynamics of the interaction and effectively suppressing the BKT transition. However, this smearing of BKT physics does not significantly impact the SC state, that remains preserved, particularly in the weak field regime, allowing for a selective control of fluctuation effects.

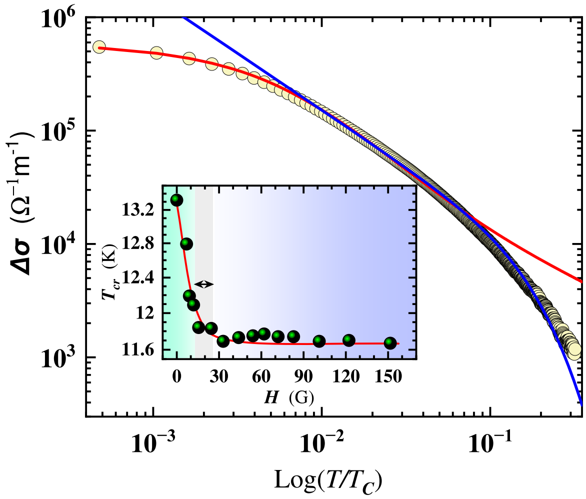

Fig. 5. a) Paraconductivity of MO10 as a function of the reduced temperature, under an applied field of $H = 0$ G. Lines are least squares fitting derived by the Aslamazov-Larkin (blue, Eq. (1)) and Halperin-Nelson (red, Eq. (2)) equations. Inset. H-field dependence of the crossover temperature, T_{cr}, defined as the crossing point of the Aslamazov-Larkin and Halperin-Nelson least square fitting curves by Eqs. (1) and (2), respectively. The quite narrow crossover region from the BKT physics (pale green) to the BCS-like GL physics (pale blue) has been highlighted by a gray filled area (centred at ≃ 20 G and ≈ 15 G wide). The red line is a guide for the eye.

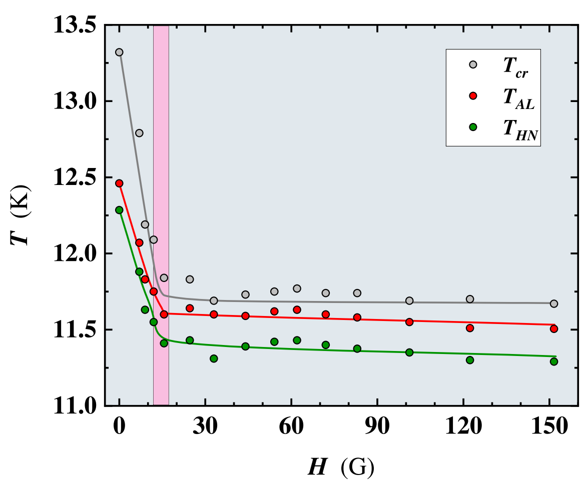

Fig. 6. H field intensity dependence of the characteristic temperature scales of film MO10, derived by: T_{cr}, the crossing of the two fitting paraconductivity equations [(Eqs. (1) and (2), in the main text]; T_{AL}, the Aslamazov-Larkin critical temperature; T_{HN}, the Halperin-Nelson critical temperature (for a definition of these temperatures see the Supplementary Material). The pink filled rectangle highlights the crossover region. The lines are guides to the eye.

A detailed analysis of the paraconductivity of films exhibiting the BKT effect, revealed interesting findings. In particular, in the absence of any applied H field, the Halperin-Nelson approach, Eq. (2), succeeded to fit the fluctuation conductivity of a thin NbN film (MO10), in the region following the SC transition, where the BKT mechanism persists (Fig. 5).

In presence of H, the Halperin-Nelson equation starts to deviate significantly from the experimental data, with a gradual crossover from the Halperin-Nelson to the Ginzburg-Landau (GL) description, as evidenced by the progressive decrease in the crossover temperature, T_{cr} (Fig. 5, inset), defined as the temperature at which the crossover between the Halperin-Nelson and the Aslamazov-Larkin fitting functions of the paraconductivity takes place. Therefore, the value of T_{cr} enabled

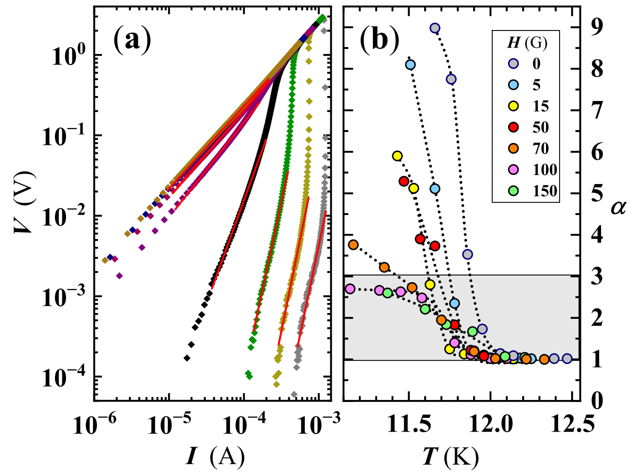

Fig. 7. a) $V - I$ curves of MO10, at several T close to T_C, under an applied field of $H = 5$ G. Red lines are least square fitting by the relation $V \propto I(T)^{\alpha(T)}$ of curves measured at (from right to left): 11.30 K, 11.43 K, 11.53 K, 11.63 K, 11.75 K, 11.84 K, 12.0 K, and 12.14 K. A similar behavior has been detected at higher H field intensities up to 150 G. b) Temperature dependence of the fitted α exponent for several H field intensities. Dotted lines are guides to the eye.

us to identify the H field-induced crossover from BKT physics to GL physics (Fig. 5, inset). These findings align with the observations made regarding the behavior of T_c for MO10 (see Fig. 2). We detect a progressive lowering of T_{cr}, allowing to identify the H-field-driven crossover at $H \approx 15 - 20$ G from the BKT to the GL physics (Fig. 5, inset), in agreement with findings of T_c behavior of sample MO10.

A H field dependent behavior similar to that found in T_{cr} is observed in the critical temperatures T_{AL} and T_{HN}, fitting parameters of the Aslamazov-Larkin and Halperin-Nelson equations, respectively (Fig. 6). We wish to point out that the fitting procedure has been carried on each curve with two different equations in two different T regions. The smooth overlap of the two fitting curves in the crossover region (see the blue and red lines in Fig. 5) and the similar H field dependence of the accounted critical temperatures, confirm the validity and robustness of our analysis and conclusions. The fact that the temperature scales T_{cr}, T_{AL} and T_{HN} mirror the behavior of T_c, suggests that the internal mechanisms ruling the shift between T_{AL} and T_{HN}, and the crossover from one fluctuation regime to the other, are weakly affected by the magnetic field. Indeed, as pointed out before $T_{AL} - T_{HN} \approx 0.2$ K stays constant with changing H (Table 1). As far as we can understand, this outcome could not be anticipated, and will certainly constrain and guide the elaboration of a microscopic model that captures the phenomenology uncovered by our work.

As previously stated, a distinctive feature of the BKT transition is the discontinuous jump in the superfluid stiffness, J_S. Therefore, it is interesting to assess its occurrence in presence of a magnetic field. Typically, the discontinuous jump in J_S is determined by two distinct approaches: direct measurement of the inverse penetration depth [25] and indirect measurement of the exponent, $\alpha(T)$, derived from the non-linear behavior of $I - V$ characteristics near T_c. Both approaches result into similar outcomes, as investigated by Venditti et al. [25]. Here, we follow the latter approach. The power law dependence is given by $V \propto [I(T)]^{\alpha(T)}$, where the exponent $\alpha(T) = 1 + \pi J_S(T)/T$ is determined from the slope of the $I - V$ characteristics in a log-log plot, measured at several temperatures close to T_c, under various H fields (Fig. 7a).

The branch of the $I - V$ used to extract α, while still evident, tends to reduce progressively at higher H intensity. Experimentally, the main problem is the correct identification of the temperature range and the current intensity of applicability of the relation $\alpha(T) = 1 + \pi J_s(T)/T$ that, as mentioned above, must be below T_{BKT} and above an intensity

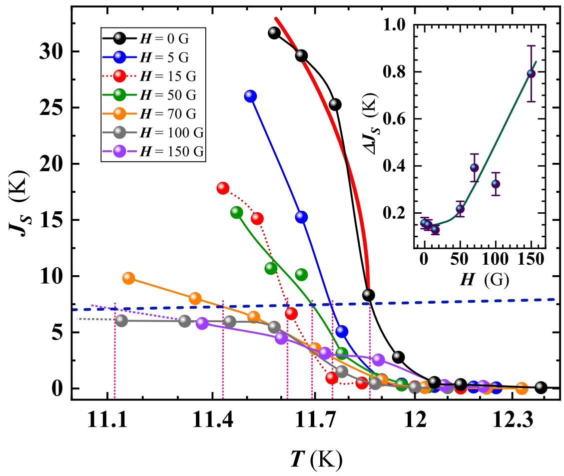

Fig. 8. Temperature dependence of the SC stiffness of MO10, derived from $\alpha(T)$ measured at several H field intensities (see Fig. 7b). Data at $H = 0$ G were fitted using Eq. (4) for $T \leq T_{BKT} = 11.86$ K, value resulting by the intersection of the $2T/\pi$ line (blue dashed) with the interpolated J_S curve (black line). The fit yields $A = 10.4 \pm 0.6$ K$^{-1/2}$. Solid lines are modified Bezier lines, guides to the eye. Inset: Magnetic-field dependence of the J_S transition width, estimated as the temperature difference between 10% and 90% of the J_S reference values, defined as the intercept between the $2T/\pi$ line and the curves interpolating the experimental J_S data (vertical dotted lines). The solid line is a guide to the eye.

threshold I^*, that Benfatto et al. [5] found to be:

$$I^* = \frac{c}{\Phi_0} 4k_B T_{\mathrm{BKT}} \approx 2.67 \times 10^{-8}\, T_{\mathrm{BKT}}. \quad (3)$$

Considering that $c/\Phi_0 = 5 \times 10^{14}$ A/J and in conventional superconductors $T_{\mathrm{BKT}} \approx 10$ K, the I^* value results of the order of 10^{-7} A. However, experimental studies have reported a higher intensity, of the order of 10^{-5} A, due to the inhomogeneity effects, as well documented and explained in ref. [5].

From our analysis, we found a sizable H dependence of $\alpha(T)$. At intensities as low as 5 G, α is downward shifted and starts to lower its slope (Fig. 7b). The shift continues up to 15 G, while at $H > 50$ G, a sizable lowering of the slope starts to occur, together with a discontinuous change in α (Fig. 7b). At 100 G, increasing T up to 11.6 K, α saturates at a value of ≈ 2.5, to finally converge to $\alpha = 1$ at $T \approx 12$ K. As it is known, at $T = T_{\mathrm{BKT}}$, J_S is expected to jump discontinuously, from $J_S(T^-_{\mathrm{BKT}}) = 2T_{\mathrm{BKT}}/\pi$ to $J_S(T^+_{\mathrm{BKT}}) = 0$, giving $\alpha(T^-_{\mathrm{BKT}}) = 3$ and $\alpha(T^+_{\mathrm{BKT}}) = 1$, respectively.

To gain more insight into the smearing of the BKT transition with increasing H, we have derived $J_S(T)$ close to the SC transition (Fig. 8) from the extracted α values by using the relation $J_S(T) = [\alpha(T) - 1]T/\pi$ [25]. In the case of $H = 0$, J_S shows quite an abrupt jump at T_{BKT} and its T dependence before the transition has been fitted by the functional dependence of the renormalization group equations given by:

$$J_S(T) = \frac{2T}{\pi} + \frac{4AT}{\pi^2}\sqrt{T_{\mathrm{BKT}} - T} \quad (4)$$

where the fitted parameter is $A = 10.4 \pm 0.6$ K$^{-1/2}$. The agreement between experiment and theory is satisfactory (Fig. 8), pointing toward an accurate BKT description of the SC transition at zero field. Increasing H, the fit fails and the sharpness of the jump starts to smear. To account for this smearing, we have estimated the J_S width, ΔJ_S, of the jump, starting from the intersection with the universal line $2T/\pi$. The trend of ΔJ_S vs H, further confirms the progressive smearing of the BKT physics with increasing H (Fig. 8, inset).

In conclusion, our study demonstrates that the BKT transition in NbN ultra-thin films exhibits an exceptionally high sensitivity to weak perpendicular magnetic fields. Our experimental results show that clear signatures of BKT physics persist up to $H \simeq 5$ G. Upon increasing the magnetic field to approximately 15–20 G, the system undergoes a crossover from a BKT-dominated regime to a BCS-like SC transition. The existence of such a crossover regime is further corroborated by the progressive breakdown of the Halperin-Nelson description of the fluctuation conductivity near the BKT transition with increasing H, accompanied by a markedly improved agreement between the experimental data and the Aslamazov-Larkin formalism. This behavior points to the emergence of GL type SC fluctuations superimposed on an underlying BCS SC state. At higher magnetic fields, $H \gtrsim 100$ G, all signatures of BKT physics are completely suppressed. We attribute this evolution to the increasing density of field-induced vortices, which screen and weaken vortex-antivortex interactions, thereby driving a tunable crossover from BKT to BCS superconductivity.

In principle, field-induced free vortices may organize into a regular lattice. However, in the very low-field regime explored in this work, the corresponding lattice periodicity is expected to exceed the characteristic length scale of structural defects, likely inhibiting the formation of an ordered vortex lattice. As the magnetic field increases, the vortex lattice becomes progressively denser and may start to influence the SC properties in the vicinity of the transition, as discussed in Refs. [42–45].

More broadly, our results highlight the crucial role played by weak magnetic fields in 2D SC systems —effects that are essentially negligible in their 3D counterparts— and underscore the importance of accounting for such phenomena in the design of integrated SC circuits. Finally, our findings suggest that analogous behavior may emerge in related superfluid systems, such as fermionic atomic gases confined to 2D pancake geometries under slow rotation, opening new perspectives for investigating BKT physics in rotating 2D superfluids.

CRediT authorship contribution statement

Meenakshi Sharma: Writing – original draft, Visualization, Validation, Resources, Investigation, Methodology, Formal analysis, Data curation; **Sergio Caprara:** Writing – review & editing, Methodology, Formal analysis, Conceptualization; **Andrea Perali:** Supervision, Methodology, Investigation, Formal analysis, Conceptualization; **Surinder P. Singh:** Resources, Investigation, Data curation; **Sandeep Singh:** Resources, Investigation, Data curation; **Matteo Fretto:** Resources, Data curation; **Natascia De Leo:** Resources, Data curation; **Nicola Pinto:** Writing – review & editing, Writing – original draft, Supervision, Methodology, Investigation, Formal analysis, Data curation, Conceptualization.

Declaration of competing interest

The authors declare that they have no known competing financial interests or personal relationships that could have appeared to influence the work reported in this paper.

Acknowledgements

We thank Giovanni Midei and Giulia Venditti for fruitful discussions. Part of the experimental activity has been carried out at QR Lab - Micro&Nanolaboratories, INRiM. This work has been partially supported by PNRR MUR Project No. PE0000023-NQSTI, PRIN 2022 MUR, Project No. 2022H77XB7, and by the ‘Ateneo Research Projects’ of the University of Rome Sapienza: ‘Models and theories from anomalous diffusion to strange-metal behavior’ (n. RM12218162CF9D05), ‘Non-conventional aspects for transport phenomena and non-equilibrium statistical mechanics’ (n. RM123188E830D258), ‘Elementary excitations at the origin of glassy or hexatic behavior in low dimensional system, at and out of equilibrium’ (n. RM124190C54BE48D).

Supplementary material

Supplementary material associated with this article can be found in the online version at 10.1016/j.supcon.2026.100256.

References

[1] Kosterlitz JM, Thouless DJ, Ordering, metastability and phase transitions in two-dimensional systems. J Phys C Solid State Phys 1973;6(7):1181.

[2] Yong J, Lemberger T, Benfatto L, Ilin K, Siegel M, Robustness of the Berezinskii-Kosterlitz-Thouless transition in ultra-thin NbN films near the superconductor-insulator transition. Phys Rev B 2013;87(18):184505.

[3] Bartolf H, Engel A, Schilling A, Il'in K, Siegel M, Hübers H-W, et al. Current-assisted thermally activated flux liberation in ultrathin nanopatterned NbN superconducting meander structures. Phys Rev B 2010;81(2):024502.

[4] Hu Z, Ma Z, Liao Y-D, Li H, Ma C, Cui Y, et al. Evidence of the Berezinskii-Kosterlitz-Thouless phase in a frustrated magnet. Nat Comm 2020;11(1):5631.

[5] Benfatto L, Castellani C, Giamarchi T, Broadening of the Berezinskii-Kosterlitz-Thouless superconducting transition by inhomogeneity and finite-size effects. Phys Rev B 2009;80(21):214506.

[6] Mondal M, Kumar S, Chand M, Kamlapure A, Saraswat G, Seibold G, et al. Role of the vortex-core energy on the Berezinskii-Kosterlitz-Thouless transition in thin films of NbN. Phys Rev Lett 2011;107(21):217003.

[7] Weitzel A, Pfaffinger L, Maccari I, Kronfeldner K, Huber T, Fuchs L, et al. Sharpness of the Berezinskii-Kosterlitz-Thouless transition in disordered NbN films. Phys Rev Lett 2023;131:186002.

[8] Franz M, Millis AJ, Phase fluctuations and spectral properties of underdoped cuprates. Phys Rev B 1998;58:14572–80.

[9] Marsiglio F, Pieri P, Perali A, Palestini F, Strinati GC, Pairing effects in the normal phase of a two-dimensional fermi gas, Phys Rev B, 2015;91:054509. https://doi.org/10.1103/physrevb.91.054509

[10] Hsu J, Kapitulnik A, Superconducting transition, fluctuation, and vortex motion in a two-dimensional single-crystal NB film. Phys Rev B 1992;45(9):4819.

[11] Caprara S, Grilli M, Leridon B, Vanacken J, Paraconductivity in layered cuprates behaves as if due to pairing of nearly free quasiparticles. Phys Rev B 2009;79(2):024506.

[12] ń RB, Mazzanti F, Boronat J, Berezinskii-Kosterlitz-Thouless transition in two-dimensional dipolar stripes. Phys Rev A 2019;100:063614.

[13] Zhang W, Lin G-D, Duan L-M, Berezinskii-Kosterlitz-Thouless transition in a trapped quasi-two-dimensional fermi gas near a feshbach resonance; Phys Rev A 2008; 78:043617. https://doi.org/10.1103/physreva.78.043617

[14] Sharma M, Singh M, Rakshit RK, Singh SP, Fretto M, Leo ND, et al. Complex phase-fluctuation effects correlated with granularity in superconducting NbN nanofilms. Nanomaterials 2022;12(23):4109.

[15] der Zant HV, Rijken H, Mooij J, The superconducting transition of 2-D josephson-junction arrays in a small perpendicular magnetic field. J Low Temp Phys 1990;79:289–310.

[16] Mironov AY, Silevitch DM, Proslier T, Postolova SV, Burdastyh MV, Gutakovskii AK, et al. Charge Berezinskii-Kosterlitz-Thouless transition in superconducting nbtin films. Sci Rep 2018;8(1):4082.

[17] Fisher DS, Flux-lattice melting in thin-film superconductors. Phys Rev B 1980;22(3):1190.

[18] Garland J, Lee HJ, Influence of a magnetic field on the two-dimensional phase transition in thin-film superconductors. Phys Rev B 1987;36(7):3638.

[19] Joshi LM, Verma A, Gupta A, Rout P, Husale S, Budhani R, Superconducting properties of NbN film, bridge and meanders. AIP Adv 2018;8(5).

[20] Lamura G, Villégier J-C, Gauzzi A, Cochec JL, Laval J-Y, Plaçais B, et al. Granularity-induced gapless superconductivity in NbN films: evidence of thermal phase fluctuations. Phys Rev B 2002;65(10):104507.

[21] Soldatenkova M, Triznova A, Baeva E, Zolotov P, Lomakin A, Kardakova A, et al. Normal-state transport in superconducting NbN films on r-cut sapphire. J Phys Confer Series 2021;2086(1):012212.

[22] Shapoval T, Stopfel H, Haindl S, Engelmann J, Inosov D, Holzapfel B, et al. Quantitative assessment of pinning forces and magnetic penetration depth in NbN thin films from complementary magnetic force microscopy and transport measurements. Phys Rev B 2011;83:214517.

[23] Il'in K, Siegel M, Engel A, Bartolf H, Schilling A, Semenov A, et al. Current-induced critical state in NbN thin-film structures. J of Low Temp Phys 2008;151:585–90.

[24] Gray K, Brorson J, Bancel PA, Resistance measurements and vortex fluctuations in two-dimensional superconducting films. J of Low Temp Phys 1985;59:529–45.

[25] Venditti G, Biscaras J, Hurand S, Bergeal N, Lesueur J, Dogra A, et al. Nonlinear $i-v$ characteristics of two-dimensional superconductors: Berezinskii-Kosterlitz-Thouless physics versus inhomogeneity. Phys Rev B 2019;100(6):064506.

[26] Minnhagen P, Kosterlitz-Thouless transition for a two-dimensional superconductor: magnetic-field dependence from a coulomb-gas analogy. Phys Rev B 1981;23(11):5745.

[27] Minnhagen P, Evidence of magnetic field scaling for two-dimensional superconductors. Phys Rev B 1984;29:1440.

[28] Minnhagen P, The two-dimensional coulomb gas, vortex unbinding, and superfluid-superconducting films. Rev Mod Phys 1987;59(4):1001.

[29] Halperin B, Nelson DR, Resistive transition in superconducting films. J Low Temp Phys 1979;36:599–616.

[30] Aslamasov L, Larkin A, The influence of fluctuation pairing of electrons on the conductivity of normal metal. Phys Lett A 1968;26(6):238–9.

[31] Instruments K, Achieving accurate and reliable resistance measurements in low power and low voltage applications. White Paper 2011.

[32] Pinto N, Rezvani SJ, Perali A, Flammia L, Milošević MV, Fretto M, et al. Dimensional crossover and incipient quantum size effects in superconducting niobium nanofilms. Sci Rep 2018;8(1):4710.

[33] McNaughton B, Pinto N, Perali A, Milošević MV, Causes and consequences of ordering and dynamic phases of confined vortex rows in superconducting nanostripes. Nanomaterials 2022;12(22):4043.

[34] Engel A, Bartolf H, Schilling A, Il'in K, Siegel M, Semenov A, et al. Temperature- and field-dependence of critical currents in NbN microbridges. IOP Publishing 2008;97:012152.

[35] Joshi LM, Rout P, Husale S, Gupta A, Dissipation processes in superconducting NbN nanostructures. AIP Adv 2020;10(11).

[36] Constantino NGN, Anwar MS, Kennedy OW, Dang M, Warburton PA, Fenton JC, Emergence of quantum phase-slip behaviour in superconducting NbN nanowires: DC electrical transport and fabrication technologies. Nanomaterials 2018;8(6):442.

[37] Caprara S, Grilli M, Leridon B, Lesueur J, Extended paraconductivity regime in underdoped cuprates. Phys Rev B 2005;72(10):104509.

[38] Ryzhov V, Tareyeva E, Statistical mechanics of vortex systems in two-dimensional superconductors. Phys Rev B 1993;48(17):12907.

[39] Ryzhov V, Tareeva E, Results for the phase diagram of the vortex system in two-dimensional superconductors. Phys Rev B 1994;49(9):6162.

[40] Irz DY, Ryzhov V, Tareyeva E, First-order vortex unbinding transition in thin superconducting films. Phys Rev B 1996;54(5):3051.

[41] Carbillet C, Caprara S, Grilli M, Brun C, Cren T, Debontridder F, et al. Confinement of superconducting fluctuations due to emergent electronic inhomogeneities. Phys Rev B 2016;93(14):144509.

[42] Roy I, Dutta S, Choudhury A NR, Basistha S, Maccari I, Mandal S, et al. Melting of the vortex lattice through intermediate hexatic fluid in an a-moge thin film. Phys Rev Lett 2019;122(4):047001.

[43] Maccari I, Pokharel BK, Terzic J, Dutta S, Jesudasan J, Raychaudhuri P, et al. Transport signatures of fragile glass dynamics in the melting of the two-dimensional vortex lattice Phys Rev B 2023;107:014509. https://doi.org/10.1103/physrevb.107.014509

[44] Maccari I, Benfatto L, Castellani C, Lorenzana J, Michele CD, Fragile-to-strong glass transition in two-dimensional vortex liquids; Phys Rev Res, 2025;7:013160. https://doi.org/10.1103/physrevresearch.7.013160

[45] Zhao W, Wang Q, Liu M, Zhang W, Wang Y, Chen M, et al. Evidence for Berezinskii-Kosterlitz-Thouless transition in atomically flat two-dimensional pb superconducting films. Solid State Commun 2013;165:59–63.